In situ AFM observations of the interaction between calcite $(10\bar{1}4)$ surfaces and Cd-bearing aqueous solutions

Carlos Pérez-Garrido [a], Lurdes Fernández-Díaz [a,*], Carlos M. Pina [a], Manuel Prieto [b]

[a] *Departamento de Cristalografía y Mineralogía, Universidad Complutense de Madrid, 28040 Madrid, Spain*
[b] *Departamento de Geología, Universidad de Oviedo, 33005 Oviedo, Spain*

Abstract

In situ atomic force microscopy (AFM) observations of the interaction between calcite $(10\bar{1}4)$ surfaces and Cd-bearing aqueous solutions have been carried out, by maintaining the solutions static in the AFM fluid cell. The interaction involves the dissolution of the original surface and the simultaneous epitaxial growth of multilayer three-dimensional islands ~2.75 nm in height of Cd-rich members of the $Cd_xCa_{1-x}CO_3$ solid solution. Dissolution occurs by the retreating of steps and the formation and growth of etch pits. Both the etch pits and the multilayer islands are elongated along the $[42\bar{1}]$ direction. Such an unusual elongation direction is interpreted as a kinetic effect controlled by both the structural characteristics of the calcite $(10\bar{1}4)$ surface and the structure and elastic properties of the overgrowth. Using aqueous solutions highly concentrated in cadmium, the formation of ~2.75 nm thick islands occurs after the initial growth of a solid solution monolayer ~0.3 nm thick, which finally dissolves as the islands grow. This effect seems to be a result of the coherent strain energy accumulated in the substrate–monolayer interface. Significantly, the dissolution rate of the calcite surface decreases when the concentration of Cd^{2+} in the aqueous solution increases, suggesting that, together with co-precipitation, Cd adsorption plays an important role in the interaction process. During co-precipitation, the progressive coalescence of the Cd-rich islands results in formation of a nanometric epitaxial layer on the calcite $(10\bar{1}4)$ surface. This layer armours the substrate from further dissolution and determines the end of the process at a "partial" pseudo-equilibrium endpoint.

Keywords: Calcite; Cd; Dissolution–crystallization; Atomic force microscopy

1. Introduction

The contamination of soils, surface sediments and superficial aquatic environments by toxic metals is an important problem that reduces the quality of environmental conditions in many regions [1,2]. Given that the toxicity of a contaminant is mainly related to its bioavailability rather than to its total concentration in a certain environment [3], efficient strategies of environmental remediation focus on the reduction of contaminants bioavailability without removing them from the biosphere. In the case of toxic metals, this can be done through co-precipitation reactions that lead to the formation of sparingly soluble crystalline compounds, since the incorporation of foreign ions into the crystal lattice of these phases strongly reduces their chemical lability and bioavailability. The efficiency of different minerals as pollutant removers has been studied over the last decades [4,5]. In many cases, carbonate minerals, and particularly calcite, appear to be especially suitable for this task. Carbonates are common minerals in soils and sediments [6], and show a significant ability to uptake divalent metals via different sorption mechanisms [2,7,8]. Sorption at mineral–water interfaces may involve different types of processes that include the followings [9–11]: (1) adsorption, (2) absorption, and (3) surface precipitation. The first

* Corresponding author. Tel.: +34 91 3944881; fax: +34 91 3944872.
E-mail addresses: carlospgarrido@geo.ucm.es (C. Pérez-Garrido), lfdiaz@geo.ucm.es (L. Fernández-Díaz), cmpina@geo.ucm.es (C.M. Pina), mprieto@geol.uniovi.es (M. Prieto).

one, adsorption, can involve the loss of one or more hydration water molecules by the adsorbate to form relatively strong chemical bonds with the mineral surface at specific positions. When this occurs, the process is referred to as specific adsorption or chemisorption. However, if the adsorbed specie is bounded to the mineral surface only through longer-range Coulomb forces and/or hydrogen bonding, adsorption can also be non-specific. On the other hand, absorption involves the incorporation of the sorbate into the crystal lattice of the original mineral. This mainly occurs by solid-state diffusion. This process can play an important role in the sorption of metals by minerals with open structures as zeolites [12]. However, its significance is very limited in the case of carbonate minerals, especially under room temperature conditions. Finally, mineral–aqueous solution interactions can lead to the precipitation on the mineral surface of an adherent layer of sorbate. When such a sorbate incorporates into its structure chemical species that directly come from the aqueous solution but also from the dissolution of the mineral, the process is described as co-precipitation. Frequently, co-precipitation leads to the formation of solid solutions. In this case, the similarity in the charge and size between the ad-ions and the ions derived from the dissolution of the mineral allow that both occupy the same crystallographic positions in the structure of the precipitate.

Among toxic metals, the contamination of natural and agricultural environments by Cd is especially a problem as this metal easily incorporates into the alimentary cycle, posing serious consequences on the public health. For this reason, considerable experimental work on the interaction of cadmium with the rhombohedral calcium carbonate, calcite, can be found in the geochemical literature [2,13–23]. Numerous investigators have studied the sorption rate of divalent metals onto calcite, invariably observing a rapid initial removal followed by a much slower uptake. In these investigations, different approaches have been followed: macroscopic studies using stirred flow-through or batch reactors and, more recently, microscopic studies combining high resolution methods for in situ surface imaging and analysis. The fast initial uptake is frequently interpreted as being the result of chemisorption, whereas the following slow removal is assumed to represent surface precipitation or co-precipitation [2,13,15]. In the case of cadmium, it is generally admitted from microscopic observations that long-term uptake by calcite occurs via surface precipitation of a Cd-bearing solid solution [20,21,23]. Recent publications by Prieto et al. have compared the ability of the $CaCO_3$ polymorphs calcite and aragonite to remove Cd^{2+} from polluted waters [10,24]. These authors carried out macroscopic experiments, showing that when fragments of calcite crystals are placed in contact with Cd-bearing aqueous solutions, the concentration of this metal decreases very rapidly during short periods of time, after which calcite surfaces become inefficient to uptake Cd^{2+}. Such behavior contrasts with the high uptake capacity observed when aragonite fragments are used and is interpreted as a consequence of the progressive passivation of the calcite surface. In both cases, the long-term uptake of cadmium seems to occur through a similar dissolution–crystallization mechanism, the outcome being virtually the same, that is, surface precipitation of Cd-rich members of the $Cd_xCa_{1-x}CO_3$ solid solution with a calcite type structure [25]. In the case of calcite, however, the substrate and precipitate are isostructural and the process occurs by oriented overgrowth of thin lamellar crystallites, which spread to cover the surface by an epitaxial layer. This thin layer armours the substrate from further dissolution, so that the process stops when only a small amount of cadmium has been removed from the fluid. A similar behavior has been observed upon the transformation of aragonite and calcite in contact with Mn^{2+}-bearing solutions [7].

In this paper, we present an AFM study of the interaction between calcite $(10\bar{1}4)$ surfaces and Cd-bearing aqueous solutions. The study aims to provide a better understanding of the mechanisms of Cd-uptake by calcite observed in previous papers, using in situ observations of the process on a nanoscale. The goals are: (1) to characterize the nanoscale features of the calcite dissolution process in the presence of cadmium, (2) to study the nanoscale features of the Cd-rich overgrowth and its structural relationships with the substrate, and (3) to evaluate the thickness of the overgrowing layers under different conditions, in order to establish the constraints that limit the Cd-uptake capacity of calcite.

2. Physicochemical background

Calcite ($CaCO_3$) and otavite ($CdCO_3$) are the end-members of a complete solid solution [16,25,26]. Both end-members crystallize in the rhombohedral $R\bar{3}c$ space group, with lattice parameters (using the hexagonal axial system) $a_0 = 4.9896$ Å and $c_0 = 17.061$ Å for calcite [27] and $a_0 = 4.923$ Å and $c_0 = 16.287$ Å for otavite [28]. Although there are some debates about the ideal or non-ideal character of this solid solution, most data seem to indicate that Cd^{2+} exhibits close to ideal behavior when substituting for Ca^{2+} in calcite [16]. In solid solution–aqueous solution (SS–AS) systems, the equilibrium relationships between the solid and the aqueous phases can be described by the Lippmann model [29,30]. Fig. 1 shows the Lippmann diagram for the $Cd_xCa_{1-x}CO_3$–H_2O system, where the so-called *solidus* and *solutus* curves are represented. *Solidus* and *solutus* express the total solubility product at equilibrium, $\sum \Pi_{eq}$ (i.e. the sum of the partial solubility products contributed by individual end-members of the solid solution), as a function of the solid and aqueous phase compositions, respectively. In the present case, the very high difference between the solubility products of calcite ($K_{sp} = 10^{-8.48}$, [31]) and otavite ($K_{sp} = 10^{-12.1}$, [32]) determines that the *solidus* and *solutus* curves plot very far apart. Thus, the compositions of the solid and aqueous phases coexisting at equilibrium (connected by tie lines in the diagram) differ

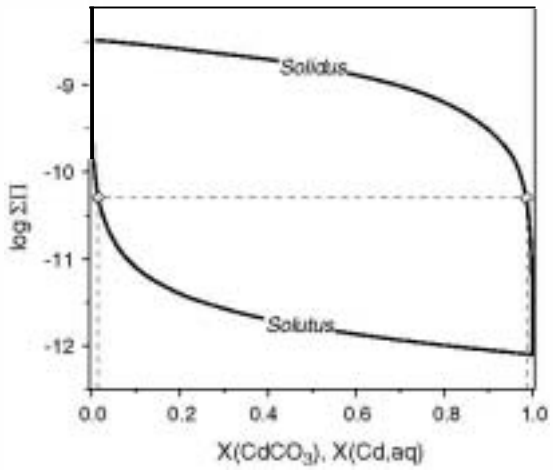

Fig. 1. Lippmann diagram for the $Cd_xCa_{1-x}CO_3$ H_2O system at 25°C. The *solidus* and *solutus* curves are represented on the ordinate versus $X(CdCO_3)$ (solid mole fraction) and $X(Cd,aq)$ (aqueous activity fraction) on the abscissa, respectively. The tie line connects a solid mole fraction with its corresponding aqueous activity fraction at thermodynamic equilibrium.

greatly, i.e. extremely Cd-rich solid solutions are in equilibrium with extremely Cd-poor aqueous solutions. This strong preferential partitioning of cadmium towards the solid phase implies that in order to precipitate a Ca-rich solid solution, the aqueous solution has to be essentially free of Cd^{2+}. Moreover, the solids forming in this SS–AS system tend to be either Ca-rich or Cd-rich over a very small range of aqueous compositions [33,34]. However, it is worth noting that under not equilibrium conditions and particularly at enhanced precipitation rates, the partition coefficient decreases and may approach unity at very high rates [35].

While Lippmann's diagrams are the most useful tool in describing equilibrium, in order to interpret crystal growth processes it is necessary to evaluate the supersaturation of the aqueous solution with respect to the solid phases that are susceptible to precipitate. This means that, in dealing with an SS–AS system, the supersaturation of a particular aqueous solution has to be calculated with respect to the whole range of solid-solution compositions. Several expressions have been derived with this aim [36,37], the simplest one being the so-called stoichiometric supersaturation, $\beta(x)$ [36]. For the case of the $Cd_xCa_{1-x}CO_3$–H_2O system, the stoichiometric supersaturation function can be expressed by

$$\beta(x) = \frac{a(Cd^{2+})^x a(Ca^{2+})^{(1-x)} a(CO_3^{2-})}{(K_{otavite} X_{CdCO_3})^x (K_{calcite} X_{CaCO_3})^{(1-x)}} \quad (1)$$

where $a(Cd^{2+})$, $a(Ca^{2+})$ and $a(CO_3^{2-})$ are the activities in the aqueous phase, $K_{otavite}$ and $K_{calcite}$ are the solubility products of the end-members of the solid solution, and X_{CdCO_3} and X_{CaCO_3} are the molar fractions of the components $CdCO_3$ and $CaCO_3$ in the solid phase. This function has a maximum, β_{max}, that represents the solid composition for which the aqueous solution is most supersaturated. Since stoichiometric saturation is a pseudo-equilibrium state [31], stoichiometric supersaturation does not represent the strict thermodynamic supersaturation, which in fact needs two equations to be described [37]. However, the function $\beta(x)$ has three particular values that represent a precise thermodynamic supersaturation: $\beta(0)$, $\beta(1)$, and β_{max} [38]. Thus, the value of x corresponding to β_{max} represents the solid solution composition for which the aqueous solution is (in the strict sense) most supersaturated and Eq. (1) can be used to find this value.

3. Experimental procedure

Natural optically clear calcite crystals (Iceland spar quality) were cleaved on $(10\bar{1}4)$ and placed inside the fluid cell of an AFM (Digital Instruments Nanoscope III Multimode). The solutions were prepared a few minutes before the beginning of each experiment, using $CdCl_2 \cdot 2.5H_2O$ (Merk, reactive grade) and deionized (Milli-Q) water. Their pH was measured using a CRISON GLP 21 pH-meter. In all the cases, the initial pH was 5.65 ± 0.05. In order to ensure the cleaning of the cleaved surface and to adjust the AFM parameters, deionized (Milli-Q) water was passed over the crystal before each experiment. Then, the fluid cell was filled with an aqueous solution containing Cd^{2+}, which was maintained static in the cell with no flow through the system. Consequently, the composition of the aqueous solution evolves as the system moves towards equilibrium. All the AFM images shown in this work were taken in constant force mode while displaying both cantilever height and deflection signals. Silicon nitride tips (Veeco NP-S10) with a nominal force constant $k = 0.06$–0.58 N/m were used. Measurements on sequences of AFM images recorded at intervals of 50–60 s allowed us to quantify nanotopographic changes that occurred during the interaction of calcite $(10\bar{1}4)$ surfaces with Cd-bearing solutions. The initial compositions of the aqueous solutions and the length of the experiments (>60 min) are shown in Table 1. An additional set of measurements was carried out with pure water, in order to obtain reference data under similar conditions (without flow through the fluid cell after the first injection) to those used in the experiments of Table 1. All the experiments were conducted at room temperature.

Table 1
Initial concentration of the aqueous solution and length of the experiments

Experiment	$CdCl_2$ (mM)	Experiment length (min)
1	0.05	90
2	0.025	120
3	0.01	60
4	0.005	150

4. Results

4.1. Dissolution of calcite $(10\bar{1}4)$ surfaces in the presence of Cd^{2+}

In contact with pure water, the calcite $(10\bar{1}4)$ surface undergoes a dissolution process that is characterized by the formation and rapid coalescence of etch pits and by the retreat of the original cleavage steps. The etch pits show a characteristic rhombus shape, bounded by $[\bar{4}41]$ and $[48\bar{1}]$ edges (Fig. 2a). Since dissolution occurs under static conditions (i.e. without flow-through the fluid cell), the system progressively approaches saturation with respect to calcite. Consequently, the measured dissolution rates decrease along time, until the process finally stops. Apart from this, our results coincide with previous observations by other authors [39-42]. It is worth noting that, in spite of this change in the dissolution rate, the etch pits maintain their typical rhombus shape, the $[42\bar{1}]/[010]$ length ratio remaining constant and close to 0.7 during the whole dissolution process (see caption of Fig. 2).

In the presence of Cd-bearing aqueous solutions, the etch pits modify their shape, progressively adopting a pseudo-elliptical morphology. When new etch pits nucleate on the surface, their shape initially coincides with that shown by etch pits formed in contact with pure water, with an initial $[42\bar{1}]/[010]$ length ratio of ~0.7. However, as dissolution progresses, the etch pits become elongated along $[42\bar{1}]$, progressively approaching a $[42\bar{1}]/[010]$ length ratio close to 2.4 (see Fig. 3). Such morphological evolution goes together with a clear roughening of the etch pits edges, which become scalloped. The progressive roughening of the edges determines the loss of the angles in the original rhombus. Only the obtuse angle defined by $[\bar{4}41]_-$ and $[48\bar{1}]_-$ remains identifiable during the expansion of a given etch pit. Moreover, the etch pits develop new straight edges, approximately parallel to $[42\bar{1}]$, i.e. to the elongation direction. Due to the irregular contour of these pits, their expansion rate has not been measured from the advancement of the typical $[\bar{4}41]$ and $[48\bar{1}]$ rhombohedral edges, but from the variation in length of the two main diagonals ($[42\bar{1}]$ and $[010]$) of the rhombus that these edges define (see Fig. 2a). This allows comparing the observations carried out in pure water with those carried out in solutions containing different initial Cd^{2+} concentrations.

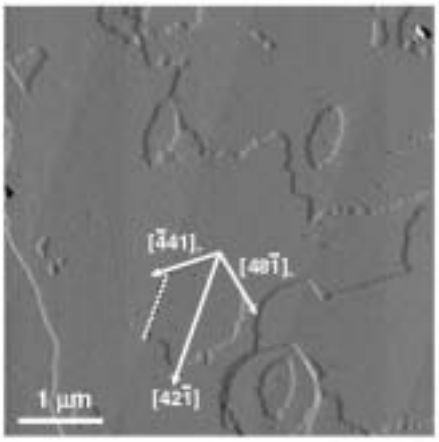

Fig. 3. Calcite $(10\bar{1}4)$ surface after dissolving for 5 min in contact with a Cd-bearing (0.025 mM) aqueous solution. The etch pits are elongated along $[42\bar{1}]$ and show straight steps parallel to $[\bar{4}41]_-$ and $[48\bar{1}]_-$ near the corner that they define. The rest of the edges appear scalloped and rough, although new edges parallel to $[42\bar{1}]$ merge (dashed line).

In contact with pure water, the length of the rhombus diagonals $[42\bar{1}]$ and $[010]$ initially increases at a rate of 0.7 nm/s and 1.0 nm/s, respectively. Then, the progress of dissolution approaches the solution to saturation with respect to calcite, which determines a progressive decrease of the expansion rate. Thus, after a period of 45 min, the etch pits expand at 0.3 nm/s along $[42\bar{1}]$ and 0.4 nm/s along $[010]$. Differently, in the presence of Cd^{2+}, the expansion rates depend on the initial concentration of

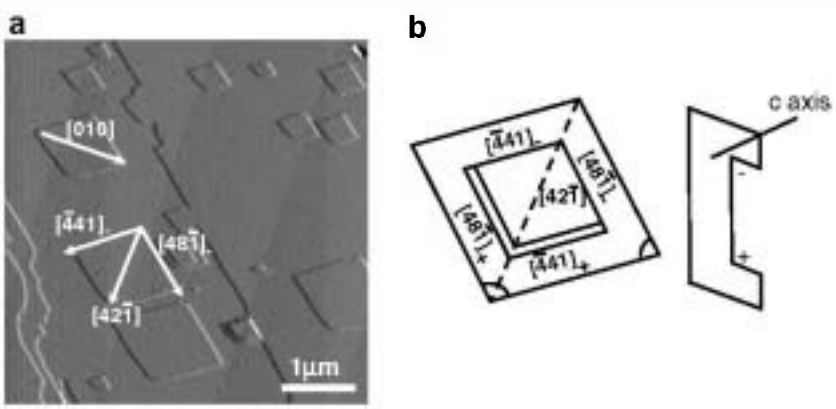

Fig. 2. (a) Calcite $(10\bar{1}4)$ surface dissolving in pure water. Steps at pits are oriented parallel to the rhombohedral $[\bar{4}41]$ and $[48\bar{1}]$ directions, defining a rhombus shape. The long and the short diagonals of the rhombus run parallel to $[010]$ and $[42\bar{1}]$, respectively. (b) Sketch of the $(10\bar{1}4)$ cleavage surface of calcite, showing the orientation and notation of steps in an etch pit, and section along $[42\bar{1}]$, showing the acute and obtuse parallel steps. It is worth noting that the rhombus diagonal $[42\bar{1}]$ is frequently indexed in the scientific literature as $[2\bar{2}1]$. This last indexation is incorrect since $[2\bar{2}1]$ direction is not in plane $(10\bar{1}4)$, but in $(\bar{1}104)$, a symmetry-equivalent plane of the crystal form $\{10\bar{1}4\}$.

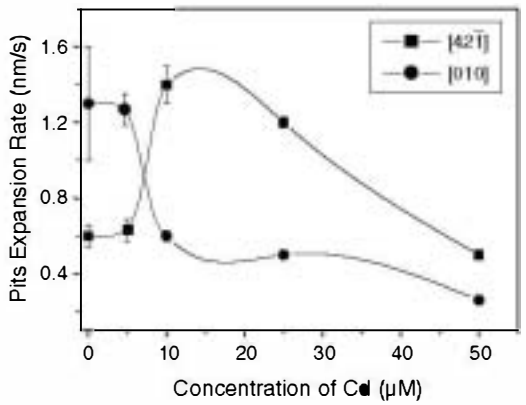

Fig. 4. Expansion rates of the etch pits along [42$\bar{1}$] and [010] as a function of the initial Cd^{2+} concentration in the aqueous solution. The values correspond to the first 10 min of interaction.

Cd^{2+} in the aqueous solution. In all the cases considered, the expansion rates are high during the first minute, but fall down rapidly. Moreover, two aspects deserve special attention: (1) While in pure water the length of the etch pits along [010] grows more rapidly than along [42$\bar{1}$], in contact with Cd-bearing solutions the opposite occurs. Such reversed behavior can be observed in Fig. 4, which shows the average expansion rates along these directions after ~10 min of dissolution. (2) The expansion rates slow down much more rapidly in the presence of Cd^{2+} and this behavior becomes more evident when higher Cd^{2+} concentrations are used. Thus, in contact with Cd^{2+} 0.05 mM solutions, the dissolution rate along both directions reaches a value close to zero after a short period (~15 min). On the contrary, using a 0.01 mM solution, the dissolution rate reaches a value of 0.6 ± 0.06 nm/s along [42$\bar{1}$] and of 0.2 ± 0.04 nm/s along [010] that remains approximately constant for a period of about 30 min.

4.2. Nucleation and growth processes during the interaction between calcite (10$\bar{1}$4) surfaces and Cd-bearing aqueous solutions

Dissolution is accompanied by nucleation of a new phase on the calcite surface, after a period that depends on the initial concentration of Cd^{2+} in the solution. This period ranges from approximately 4 min when the initial Cd^{2+} concentration is 0.05 mM to 20 min when it is 0.005 mM. Independently of the initial Cd^{2+} concentration in the aqueous solution, the nuclei reach a thickness of 2.75 ± 0.25 nm during the very early stages of their formation (Fig. 5a and b). Hereafter these nuclei will be referred to as three-dimensional islands, in agreement with the term used by Chernov [43] to describe epitaxial growth. The growth of the three-dimensional islands occurs by lateral advancement, without significant increase of their height that remains approximately constant during the whole

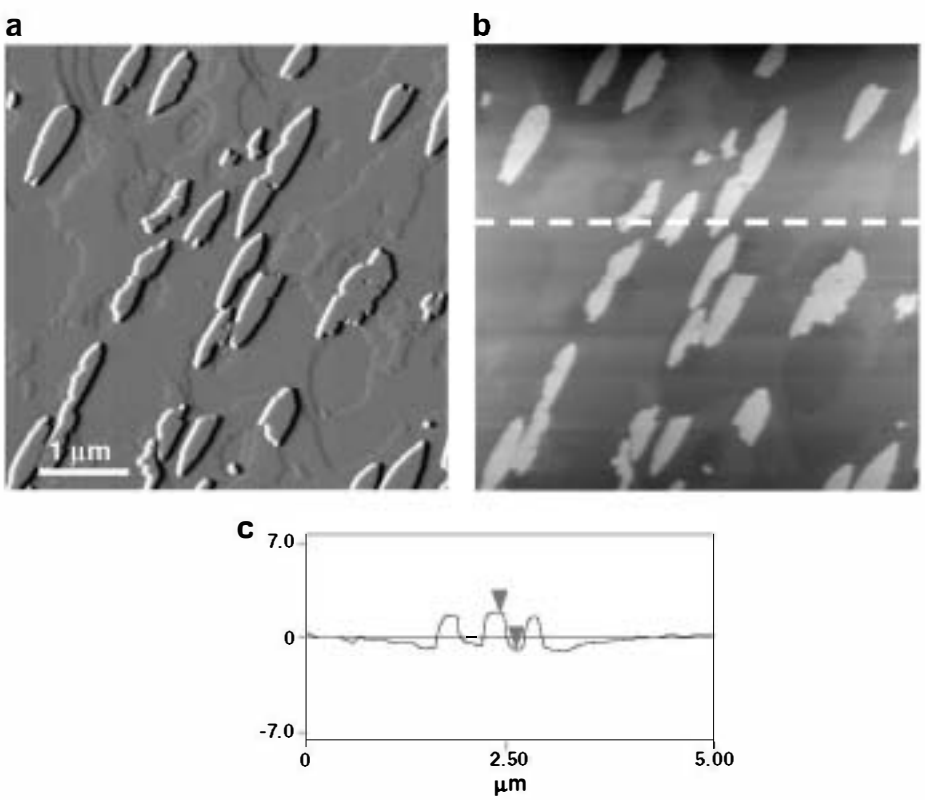

Fig. 5. (a) AFM deflection image showing three-dimensional islands growing on a calcite surface in contact with a 0.025 mM $CdCl_2$ solution. The islands grow elongated along [42$\bar{1}$]. (b) Height AFM image corresponding to the same area. (c) Height profile along the dashed line in (b). The vertical distance between the triangular indicators is 2.76 nm.

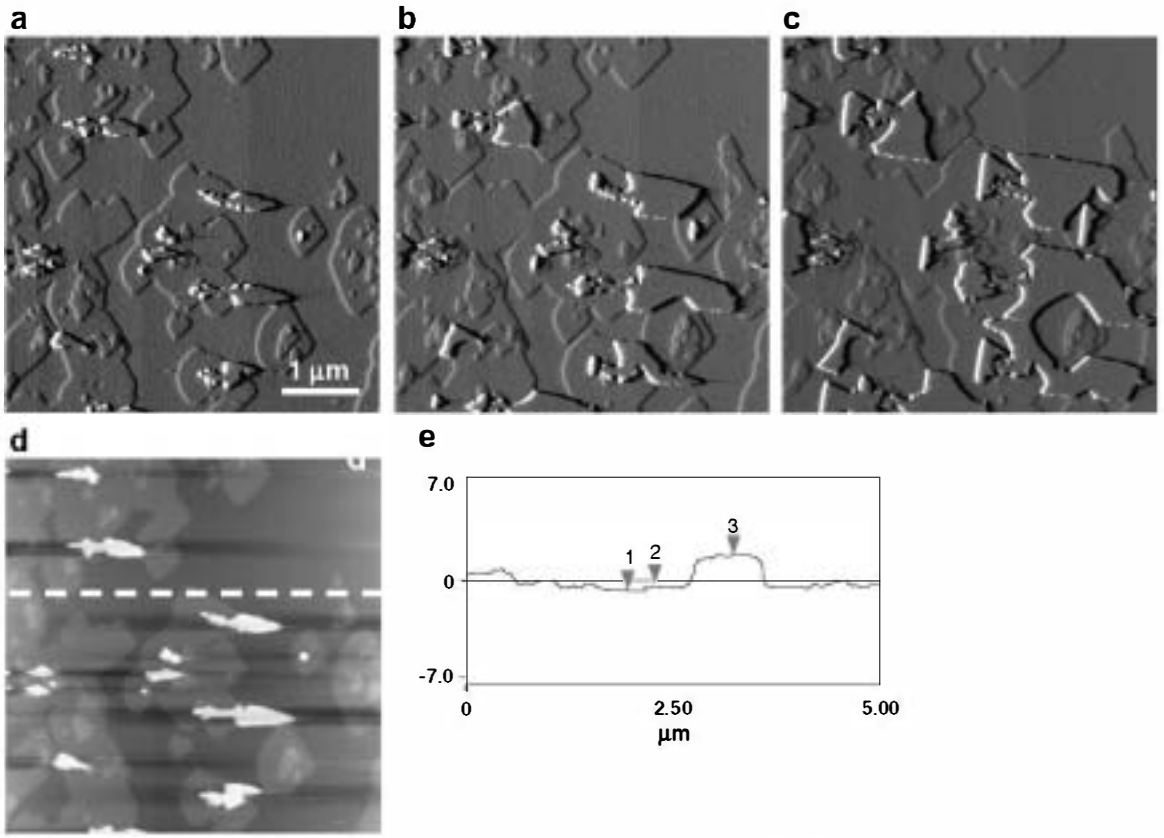

Fig. 6. (a c) Sequence of AFM deflection images showing the spread of a monolayer on a calcite $(10\bar{1}4)$ surface, simultaneously to the formation of three-dimensional islands on such monolayer. The monolayer almost completely covers the calcite substrate. The coalescence of the three-dimensional islands leads to the formation of a homogeneous "crust" that appears as large patches on the surface. (d) Height AFM image showing the formation of thick islands on top of the monolayer. (e) Height profile along the dashed line in (d). The vertical distance between the triangular pointers 2 and 3 indicates the height of a three-dimensional island, ~2.6 nm. The distance between 1 and 2 indicates the height of a monolayer, ~2.9 Å. Parent solution: 0.05 mM $CdCl_2$.

growth process. Independently of the initial concentration of Cd^{2+} in the solution, the islands show a characteristic elongated shape, without well-defined straight edges (Fig. 5a). Moreover, these islands appear oriented with respect to the calcite $(10\bar{1}4)$ surface, with their long axis parallel to $[42\bar{1}]$ and the short one parallel to $[010]$.

When aqueous solutions with high Cd^{2+} concentrations are used (0.05 mM), the growth process is, however, rather different. In such a case, two-dimensional nuclei (~0.3 nm in height) rapidly form and spread on the surface, forming a monolayer that partially covers the substrate (Fig. 6a and b). Subsequently, three-dimensional islands, 2.75 ± 0.25 nm in height, nucleate on this layer. The monolayer and the three-dimensional islands grow simultaneously until the monolayer completely covers the calcite surface, preventing further interaction with the solution. Finally, ~50 min after the formation of the first nuclei, the preliminary monolayer starts to dissolve, while the lateral growth of the three-dimensional islands continuous to progress.

Whereas the dissolution of the substrate occurs at a progressively reduced rate, the islands grow at a more or less constant rate during a period of about 30 min, after which their growth rate starts to decrease slowly. The growth rate of the islands depends on the Cd^{2+} concentration in the aqueous solution, the higher the concentration the higher the growth rate. Thus, the average growth rates along $[42\bar{1}]$, measured during the first 10 min of the growth pro-

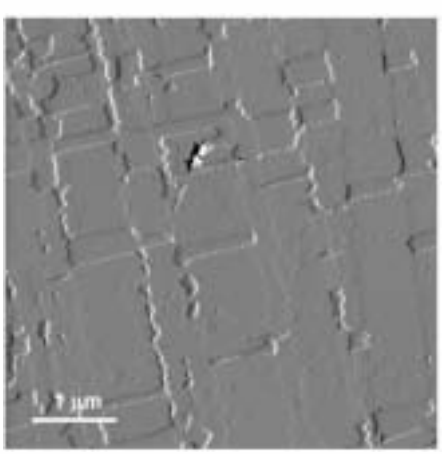

Fig. 7. AFM deflection image showing a homogeneous layer of $Cd_xCa_{1-x}CO_3$ formed on calcite $(10\bar{1}4)$ surface ~60 min after starting its interaction with a 0.025 mM $CdCl_2$ solution. The newly grown layer reproduces the original nanotopography of the calcite substrate.

cess, are 0.5 ± 0.05 nm/s for a 0.05 mM $CdCl_2$ parent solution and 0.2 ± 0.05 nm/s for a 0.005 mM parent solution. Obviously, the elongated morphology of the islands is a consequence of their highly anisotropic growth, which occurs much more rapidly along $[42\bar{1}]$ than along [010].

Eventually, the growth of the three-dimensional islands leads to their coalescence. Thus, when the initial Cd^{2+} concentration in the aqueous solution is high, a nanometric "crust" that almost completely covers the calcite $(10\bar{1}4)$ surface forms (see Fig. 7), determining the end of the process. Such "crust" reproduces the nanotopographic features (cleavage steps) of the original surface in a way that is reminiscent of the so-called "template effect", a nanoscale phenomenon previously observed in studying Mn^{2+}–calcite interactions [44].

5. Discussion

The interaction between calcite $(10\bar{1}4)$ surfaces and Cd-bearing aqueous solutions leads to a number of coupled processes, including dissolution, adsorption, and surface nucleation and growth of a nanoscopic precipitate. The described AFM observations inform on the nanotopographic expression of the mechanisms operating during these processes, but are not enough to account for the nature of these molecular-scale mechanisms. The main problem here is that while AFM is chemically "blind", other techniques do not inform about aspects like the geometry and spatial distribution of the sorbate at a nanoscale. Actually, it is generally admitted that no single technique can account for these kinds of surface processes, which need simultaneous use of several methods to be characterized. Particularly, in order to establish the actual composition of the precipitates grown on calcite surfaces as a result of the interaction with Cd-bearing aqueous solutions, the use of high resolution surface analysis techniques would be required. In this work, that kind of techniques has not been applied. However, there is ample information in the scientific literature on Cd–calcite interactions, involving different (macroscopic, microscopic, and molecular) scales and techniques [2,13–23]. This information constitutes a suitable background to interpret our AFM observations, of which the most striking are: (1) the change in the etch pits morphology in comparison with that characteristic of dissolution in pure water, (2) the decrease in the dissolution rate with the increase of the initial concentration of Cd^{2+} in the aqueous solution, and (3) the growth of elongated three-dimensional islands of constant thickness, oriented with respect to specific crystallographic directions on the calcite substrate.

5.1. Adsorption and dissolution

Numerous AFM studies have given insight into the morphology of etch pits forming on calcite $(10\bar{1}4)$ surfaces during dissolution in pure water [39–42]. All concluded that calcite structure exerts a strong control on its dissolution, with the etch pit shape defined by edges that run parallel to the most stable "periodic bond chains" (PBCs) [45–47]. Moreover, calcite dissolution is highly anisotropic, with a pair of steps moving rapidly, while the other pair retreats slowly. This is a consequence of the inequivalence of the two pairs (positive and negative) of opposing straight steps parallel to the $[\bar{4}41]$ and $[48\bar{1}]$ directions (see Fig. 2b) [47–49]. The "negative" $[\bar{4}41]_-$ and $[48\bar{1}]_-$ steps overhang the underlying layer defining an acute angle (78°) that delimits constrained kink sites. In contrast, the "positive" $[\bar{4}41]_+$ and $[48\bar{1}]_+$ steps define an obtuse angle (102°) that contains open kink sites. Obtuse (positive) steps offer greater accessibility to the solvent and, consequently, retreat much faster than acute (negative) steps.

These previous features have to be considered in order to explain the change in the etch pits' morphologies when dissolution occurs in the presence of cadmium. The first point is that, in the presence of Cd^{2+}, dissolution occurs simultaneously with adsorption and this fact necessarily affects the dissolution rate. Moreover, cadmium can be expected to be differently adsorbed at the different types of kink sites existing on $(10\bar{1}4)$, and this has to affect the etch pits' shapes.

According to our results, the expansion rates of the etch pits slow down much more rapidly in the presence of Cd^{2+} and this behavior becomes more evident when the Cd^{2+} concentration increases. This finding is not surprising, since it is well known [50] that the adsorption of impurities to kink sites can exert an inhibitory effect on mineral dissolution. Particularly, different macroscopic studies have demonstrated that, in the presence of cations that form carbonates less soluble than calcite, the dissolution of calcite becomes partially inhibited, an inverse relationship existing between the solubility of the specific metal carbonate and its effectiveness in inhibiting calcite dissolution [51]. Thus, the presence of Cd^{2+} should exert an important inhibitory effect on calcite dissolution, since the solubility product of otavite is almost four orders of magnitude smaller than that of calcite. In fact, Hay et al. [52] have reported such an inhibitory effect in a recent study, although these authors used different concentrations and pH conditions. Moreover, other cations smaller than Ca^{2+}, like Mn^{2+} and Mg^{2+}, also seem to exert a similar influence on calcite dissolution [52–54]. Our results confirm these previous findings and point out that in the case of Cd^{2+} a critical concentration value exists (~0.005 mM), below which calcite dissolution occurs at approximately the same rate as in contact with pure water. This last observation seems to be in agreement with models [50] that predict two dissolution regimes in the presence of impurities: one corresponding to low impurity concentrations, with a negligible effect, followed by a significantly affected dissolution regime at higher impurity concentrations.

The adsorption of Cd^{2+} not only affects the expansion rate of the etch pits, but also their shape. This fact has necessarily to be related to the preferential incorporation of Cd^{2+} at specific types of sites on $(10\bar{1}4)$, determining the

blocking of those sites. As previously explained, in the presence of Cd^{2+}, the etch pits lose their characteristic rhombus shape, acquiring a more or less elliptical appearance, with a long axis parallel to $[42\bar{1}]$ and a short one parallel to [010]. The calcite $(10\bar{1}4)$ surface has a strong F character and four PBCs run along $[\bar{4}41]$, $[48\bar{1}]$, $[42\bar{1}]$, and [010]. The PBCs along $[42\bar{1}]$, and [010] are rougher, more undulated and, consequently, correspond to less stable edges than the PBCs along $[\bar{4}41]$ and $[48\bar{1}]$. Thus, the etch pits formed in contact with pure water are bounded by edges parallel to these last directions, while show no edge parallel to $[42\bar{1}]$ or [010]. However, in the presence of Cd^{2+}, only the two edges parallel to $[\bar{4}41]_-$ and $[48\bar{1}]_-$ remain more or less straight (or finely scalloped) near the corner that they define (see Fig. 3). These directions correspond to the acute steps, i.e. the steps with more constrained kink sites. The fact that only that corner is preserved during dissolution in the presence of Cd^{2+}, strongly suggests that an important degree of Cd^{2+} preferential adsorption occurs in acute steps, stabilizing them with respect to dissolution. In contrast, obtuse steps dissolve faster, become coarsely scalloped, and no longer retain the $[\bar{4}41]_+$ and $[48\bar{1}]_+$ edges.

As in crystal growth processes, scalloping during dissolution is likely the morphologic manifestation of step pinning by impurity ions. Dissolved metals can affect dissolution through a blocking mechanism in which adsorbed metal ions at step edges form a fence to slow step retreat. Thus, coarser scalloping along the obtuse step edges may be indicative of more scarce incorporation of Cd^{2+} along those step edges than along acute step edges [55]. This is consistent with the idea that metal cations show preferential incorporation to obtuse or acute kinks as a function of their ion size [46,47,56]. In the case of Cd^{2+} (5% smaller than Ca^{2+}), a slight preferential incorporation to growth subsectors determined by acute steps has been observed using synchrotron X-ray fluorescence microanalysis (SXRFMA) [56] and lateral force microscopy (LFM) [52]. During dissolution, however, this selective effect is apparently more significant, probably because Cd^{2+} adsorbs in a more labile way at obtuse steps, which are more accessible to solvent.

A second feature affecting the etch pit shape is that dissolution occurs more rapidly along $[42\bar{1}]$, i.e. perpendicularly to the less stable (the most undulated) PBC, which runs parallel to [010]. Consequently, etch pits become progressively more elongated along $[42\bar{1}]$ and new edges parallel to $[42\bar{1}]$ appear. The stabilization of the $[42\bar{1}]$ step direction is also consistent with an important preferential adsorption of Cd^{2+} at acute steps. As has been pointed out by Davis et al. [57], the $[42\bar{1}]$ step edge can become stabilized by preferential inhibition of growth (or dissolution) at the (+/−) corners where obtuse (positive) and acute (negative) steps join, i.e. where regions with different types of kinks contact each other. This phenomenon was observed during growth of calcite from solutions containing Mg^{2+}, another small cation with preference for acute steps. Our observations of the evolution of the etch pits' shape in the presence of Cd^{2+} suggest that this behavior, clearly established for growth from Mg-bearing aqueous solutions, also rules for dissolution in the presence of other cations smaller than Ca^{2+}.

5.2. *Overgrowing islands: composition, morphology, and thickness*

The formation of overgrowing islands on calcite $(10\bar{1}4)$ surface can be described as the result of a co-precipitation process. Although AFM experiments do not report chemical information, from observations carried out by other methods [10,21,23] and from thermodynamic considerations, the composition of the overgrowing islands can be assumed to be close to the otavite end-member of the $Cd_xCa_{1-x}CO_3$ solid solution series. This assumption is supported by the results of the X-ray photoelectron spectroscopy (XPS) observations carried out by Chada et al. [23] on calcite $(10\bar{1}4)$ surfaces after being maintained in contact with Cd-bearing aqueous solutions during long periods (up to four weeks). Similar conclusion was attained in a prior research [21], where the formation of epitaxial crystals of $Cd_xCa_{1-x}CO_3$ on calcite was inferred from synchrotron X-ray scattering experiments. At the very beginning of the experiments, the Ca^{2+}/Cd^{2+} ratio in the aqueous solution is zero. At this point, the solution is undersaturated with respect to calcite and the substrate starts to dissolve, releasing Ca^{2+} and CO_3^{2-} ions to the aqueous solution. Under these conditions, due to the low solubility product of otavite, the aqueous solution becomes quickly supersaturated with respect to the Cd-rich members of the $Cd_xCa_{1-x}CO_3$ solid solution. Thus, nucleation occurs, consuming CO_3^{2-} and further undersaturating the solution with respect to calcite. Although the fluid cell arrangement does not allow monitoring of concentrations, we can expect that, when nucleation occurs, the $[Ca^{2+}]/[Cd^{2+}]$ ratio in the solution is at most the one corresponding to saturation with respect to calcite. This activity ratio can be calculated using the speciation code PHREEQC [58], resulting in 1.15 and 5.75 for 0.05 mM and 0.01 mM $CdCl_2$ parent solutions, respectively. According to the Lippmann diagram (Fig. 1), such $[Ca^{2+}]/[Cd^{2+}]$ ratios would determine the formation of extremely Cd-rich nuclei. The equilibrium compositions for the solids would be in the range between $X_{CdCO_3} = 0.997$, for a 0.05 mM parent solution, and $X_{CdCO_3} = 0.976$, for a 0.005 mM parent solution. Moreover, as shown in Fig. 8, the maxima (β_{max}) of the corresponding stoichiometric supersaturation functions [36] occur for solids with the compositions mentioned above. Given that all calculations have been carried out for the less favourable $[Ca^{2+}]/[Cd^{2+}]$ ratio, these results strongly support the idea that the composition of the islands is almost pure otavite in all the experiments.

The isostructural character of substrate and overgrowth explains the epitaxial orientation of the islands. Even if the islands are pure otavite, the linear lattice misfits between

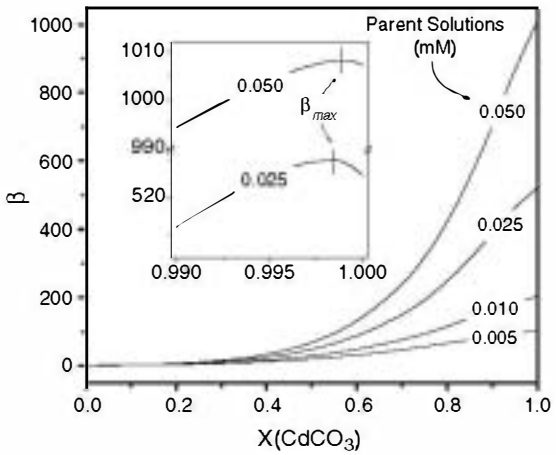

Fig. 8. Hypothetical curves of supersaturation corresponding to the aqueous solutions used in the AFM experiments. The calculation has been carried out using the initial concentrations of Cd^{2+} (Table 1) and considering the limiting case in which the $[Ca^{2+}]/[Cd^{2+}]$ ratio in the aqueous solution is the one corresponding to saturation with respect to calcite. Note that all the supersaturation maxima correspond to nearly pure otavite. The inset shows, overscaled, a detail with the exact position of the supersaturation maxima for the solutions with concentrations 0.050 mM and 0.025 mM of $CdCl_2$.

substrate and overgrowth along the PBC directions are small: 1.34% along [010], 1.97% along $[\bar{4}41]$ and $[48\bar{1}]$, 2.94% along $[42\bar{1}]$, and a slight mismatch (0.94°) in the angle between $[\bar{4}41]$ and $[48\bar{1}]$. Such a good match between both lattices is, however, contradictory with the markedly anisotropic growth of the islands. The islands show no edge parallel to $[\bar{4}41]$ and $[48\bar{1}]$, but their shape seems to be controlled by the less important PBC direction $[42\bar{1}]$. Thus, the preferred direction of growth is along the direction of greatest lattice mismatch. Lea et al. [59] have also observed the formation of islands elongated on $[42\bar{1}]$ when calcite interacts with Mn-bearing solutions. These authors interpret this fact as due in part to the decrease in elastic constant in the $[42\bar{1}]$ direction relative to the [010] direction. This could also rule for the epitaxial growth of otavite on calcite, since in calcite type structures the stiffness along $[42\bar{1}]$ is about 15% smaller than along $[\bar{4}41]$ and $[48\bar{1}]$ and ~25% smaller than along [010] [59]. A second possibility is a kinetic effect, in which the elongation on $[42\bar{1}]$ is generated by decreased growth velocities at the (+/−) corners where obtuse and acute steps join, i.e. along [010]. This effect was previously invoked to explain the change in the etch pit shapes during dissolution (see Section 5.1) and could act in a similar way during growth. Finally, there is a third possibility related to the relieving of coherency strain in the interface by generating misfit defects along $[42\bar{1}]$.

The last possibility is related to the thickness of the overgrowing islands. From the very early stages, the islands are three-dimensional, with a constant thickness of 10 monolayers. Similar thickness values have been obtained in ex situ AFM observations by other authors [23]. Thus, the spreading of these multilayer islands seems to be energetically favoured in comparison to the lateral advancement of monolayers on a substrate of different composition. This behavior is in agreement with a Volmer–Weber mechanism of epitaxy [39], which is characteristic of low adhesion between substrate and overgrowth. As we discuss below, such a weak adhesion suggests the existence of a semi-coherent rather than a completely coherent substrate–overgrowth interface. In any case, the causes of the constant thickness (2.75 ± 0.25 nm) observed in the islands are not straightforward and a suitable explanation would probably require computer simulations that are beyond the scope of the present work.

The experiments carried out with a high Cd^{2+} concentration (0.05 mM) deserve separate consideration. In this case, an otavite monolayer rapidly covers most of the calcite surface and three-dimensional islands subsequently form on this monolayer. This epitaxial growth is reminiscent of the Stranski–Krastanov mechanism [39], with the initial formation of a "wetting layer" that covers the substrate almost completely from the beginning. The Stranski–Krastanov mechanism normally indicates the existence of a stronger substrate–overgrowth adhesion than the Volmer–Weber mechanism. The point here, however, is that the operating mechanism of epitaxy seems to depend on the initial concentration of Cd^{2+} in the aqueous solution. Given that the overgrowth is of the same nature (nearly pure otavite) as in the rest of the experiments, the explanation is not straightforward and a number of phenomena could lie behind this behavior. On the one hand, the formation of a Cd-rich monolayer seems to be only possible at high supersaturation (with respect to pure otavite) reached at the initial growth stages of this (0.05 mM) experiment. On the other hand, this monolayer behaves as being metastable and tends to dissolve when the supersaturation decreases during the growth of the "more stable" three-dimensional islands. This behavior could be due to the strain energy accumulated by coherent matching between monolayer and substrate [60]. Both the small difference between lattice parameters and the fact that the monolayer inherits the growth anisotropy (the typical contour edges) of the calcite surface support this idea. In the case of the first monolayer, the coherent strain energy diminishes by surface relaxation in comparison with the strain energy accumulated when some few layers pile up [60]. Anyway, this excess energy seems to be enough to avoid the formation of a coherent monolayer in most cases. Such a monolayer only arises at high supersaturation conditions, but its growth seems to be energetically disadvantageous with respect to the growth of the coexisting semicoherent islands. Relieving the coherency strain by generating misfit defects at the interface between these islands and the calcite surface seems to be easier along $[42\bar{1}]$. This is the direction of highest misfit between both structures on the $\{10\bar{1}4\}$ surface, which moreover corresponds to an undulated, not very strong PBC.

As has been explained in Section 1, the formation of a solid solution can also be the result of absorption

processes, involving the solid-state diffusion of the adsorbate into the crystal lattice of the sorbate. Stipp et al. proposed this mechanism for the uptake and immobilization of Cd by calcite on the basis of XPS data [17]. These authors concluded that Cd diffuse, under dry conditions, over distances of nanometers from the near surface region into the bulk of calcite in a period of several days. However, other authors failed to confirm their findings using the same technique [23]. Under the conditions considered in our experiments (room temperature and interaction periods shorter than 3 h), solid-state diffusion is not a very like process to have any significance. This is supported by the calculations of Martin-Garin et al. [22], who considering a diffusion coefficient for the transfer of Cd^{2+} ions from the surface into the solid phase of 8.5×10^{-21} $cm^2\ s^{-1}$, concluded that even after periods of about 20 h, the migration of Cd^{2+} ions into calcite lattice would be limited to the outermost few Å.

5.3. *Coalescence of islands and partial equilibrium endpoints*

Given that the experiments were carried out without flow-through the fluid cell, the system should progressively approach equilibrium. However, as the interaction time passes by, the Cd-rich islands coalesce to cover the calcite surface by a layer a few nanometers thick. This thin epilayer armors the substrate from further dissolution, so that the process stops when only a small amount of cadmium has been removed from the fluid. Obviously, at this stage the system is not at equilibrium. However, the term "partial equilibrium" [61] could be used to describe a situation where the initial reacting solid becomes isolated from the aqueous solution by a coating of secondary solids that are at equilibrium with the fluid.

These nanoscopic observations are in good agreement with the macroscopic observations realized by Prieto et al. [10], who studied the decrease in cadmium concentration as a function of time in macroscopic batch experiments carried out by reacting calcite cleavage fragments with $CdCl_2$ aqueous solutions. In all the cases, these authors observed that the uptake of cadmium by calcite becomes negligible when the concentration of cadmium in the fluid is still high, which contrasts with the extremely low concentration levels that could be expected from thermodynamic calculations. After prolonged interaction periods, the aqueous solution is at equilibrium with otavite, but undersaturated with respect to calcite. This is a typical situation of partial equilibrium, in which the calcite surface is isolated from the aqueous solution and cannot dissolve. The good matching and small thickness of the epilayer observed by AFM account for these macroscopic observations.

7. Conclusions

The interaction between calcite $(10\bar{1}4)$ surfaces and Cd-bearing aqueous solutions leads to the dissolution of the original surface and the simultaneous growth of epilayers of Cd-rich members of the $Cd_xCa_{1-x}CO_3$ solid solution. The process involves nanoscale phenomena that explain previous macroscopic observations, such as the decrease of the calcite dissolution rate in the presence of Cd^{2+} or the low Cd-uptake capacity of calcite as compared with aragonite. With respect to calcite dissolution, the adsorption of Cd^{2+} not only affects the expansion rate of the etch pits, but also their shape, which become elongated on $[42\bar{1}]$ and develop a scalloped contour. These effects seem to be related to the preferential incorporation of Cd^{2+} at specific types of sites on $(10\bar{1}4)$, determining the blocking of those sites. Particularly, the stabilization of the $[42\bar{1}]$ step edge is consistent with a preferential adsorption of Cd^{2+} at acute steps and an inhibition of dissolution at the (+/−) corners where obtuse and acute steps join.

The epitaxial coating of the calcite surface occurs by coalescence of $Cd_xCa_{1-x}CO_3$ islands with a constant thickness equivalent to 10 monolayers. The islands are elongated along $[42\bar{1}]$, the direction of greatest lattice mismatch with the substrate. This apparently anomalous behavior is likely related to the elastic properties of the overgrowth and to the degree of coherency of its interface with the substrate. The occasional formation and subsequent dissolution of metastable $Cd_xCa_{1-x}CO_3$ monolayers is a result of the excess strain energy accumulated by coherent matching monolayer–substrate. More difficult to explain are the causes of the constant thickness of the islands. The obvious answer is that a 10-layer configuration of the islands is energetically advantageous, but an in-depth explanation would require computer simulations. Forthcoming papers will deal with this matter.

Acknowledgements

This work has been financially supported by projects CGL2004-02501 (Spanish Ministry of Education and Science) and 910148-Superficies Minerales (UCM-Comunidad de Madrid). Carlos Pérez-Garrido acknowledges the Spanish Ministry of Education and Science for financial support through a FPI grant. The authors thank the Centro de Microscopia (UCM) for kindly providing them access to AFM.

References

[1] L.M. Dudley, J.E. McLean, R.C. Sims, J.J. Jurinak, Soil Sci. 145 (1988) 207.
[2] J.M. Zachara, C.E. Cowan, C.T. Resch, Geochim. Cosmochim. Acta 55 (1991) 549.
[3] S.J. Traina, V. Laperche, Proc. Natl. Acad. Sci. USA 99 (1999) 3365.
[4] Y.T. He, S.J. Traina, Environ. Sci. Technol. 39 (2005) 4499.
[5] M.F. Hochella, J.N. Moore, C.V. Putnis, A. Putnis, T. Kasama, D.D. Eberl, Geochim. Cosmochim. Acta 69 (2005) 1651.
[6] R.J. Reeder, in: R.J. Reeder (Ed.), Carbonates: Mineralogy and Chemistry, Reviews in Mineralogy, vol. 11, Mineralogical Society of America, Washington, DC, 1983, p. 1.
[7] M.E. Böttcher, Mar. Chem. 57 (1997) 97.

[8] A. Godelitsas, J.M. Astilleros, K. Hallam, S. Harissopoulos, A. Putnis, Environ. Sci. Technol. 37 (2003) 3351.
[9] G. Sposito, in: J.A. Davis, K. Hayes (Eds.), Geochemical Processes of Mineral Surfaces, Symposium Series, vol. 323, American Chemical Society, 1986, p. 217.
[10] M. Prieto, P. Cubillas, A. Fernández-González, Geochim. Cosmochim. Acta 67 (2003) 3859.
[11] G.E. Brown, G.A. Parks, P. O'Day, in: D.J. Vaughan, R.A.D. Pattrick (Eds.), Mineral Surfaces, 1995, p. 129.
[12] A. Dyer, in: D.J. Vaughan, R.A.D. Pattrick (Eds.), Mineral Surfaces, 1995, p. 333.
[13] M.B. McBride, J. Soil Sci. Am. 44 (1980) 26.
[14] J.A. Davis, C.C. Fuller, A.D. Cook, Geochim. Cosmochim. Acta 51 (1987) 1477.
[15] C.C. Fuller, J.A. Davis, Geochim. Cosmochim. Acta 51 (1987) 1491.
[16] E. Könisberger, R. Hausner, H. Gamsjäger, Geochim. Cosmochim. Acta 55 (1991) 3505.
[17] S.L. Stipp, M.F. Hochella, G.A. Parks, J.O. Leckie, Geochim. Cosmochim. Acta 56 (1992) 1941.
[18] A.J. Tesoriero, J.F. Pankow, Geochim. Cosmochim. Acta 60 (1996) 1053.
[19] R.J. Reeder, Geochim. Cosmochim. Acta 60 (1996) 543.
[20] R.P. Chiarello, N.C. Sturchio, Geochim. Cosmochim. Acta 58 (1994) 5633.
[21] R.P. Chiarello, N.C. Sturchio, J.D. Grace, P. Geissbuhler, L.B. Sørensen, L. Cheng, S. Xu, Geochim. Cosmochim. Acta 61 (1997) 1467.
[22] A. Matin-Garin, P. Van Cappellen, L. Charlet, Geochim. Cosmochim. Acta 67 (2003) 2763.
[23] V.G.R. Chada, D.B. Hausner, D.R. Strongin, A.A. Rouff, R.J. Reeder, J. Colloid Interface Sci. 288 (2005) 350.
[24] P. Cubillas, S. Köhler, M. Prieto, C. Causserand, E.H. Oelkers, Geochim. Cosmochim. Acta 69 (2005) 5459.
[25] M.E. Böttcher, P.L. Gehlen, Appl. Spectrosc. 51 (1997) 130.
[26] L.L.Y. Chang, W.R. Brice, Am. Mineral. 56 (1977) 338.
[27] H. Effenberger, K. Mereiter, J. Zemann, Z. Kristallogr. 156 (1981) 233.
[28] V.L. Borodin, V.I. Lyutin, V.V. Ilyukhin, N.V. Belov, Sov. Phys. Dokl. 24 (1979) 226.
[29] F. Lippmann, Phase diagrams depicting the aqueous solubility of binary mineral systems, Neues Jb. Miner. Abh. 139 (1980) 1.
[30] P.D. Glynn, E.J. Reardon, Am. J. Sci. 290 (1990) 164.
[31] L.N. Plummer, E. Busenberg, Geochim. Cosmochim. Acta 46 (1982) 1011.
[32] S.L. Stipp, G.A. Parks, D.K. Nordstrom, J.O. Leckie, Geochim. Cosmochim. Acta 57 (1993) 2699.
[33] M. Prieto, A. Fernández-González, A. Putnis, L. Fernández-Díaz, Geochim. Cosmochim. Acta 61 (1997) 3383.
[34] A. Fernández-González, M. Prieto, A. Putnis, S. López-Andrés, Mineral. Mag. 63 (3) (1999) 331.
[35] M.E. Böttcher, Mar. Chem. 62 (1998) 287.
[36] M. Prieto, A. Putnis, L. Fernández-Díaz, Geol. Mag. 130 (1993) 289.
[37] J.M. Astilleros, C.M. Pina, L. Fernández-Díaz, A. Putnis, Geochim. Cosmochim. Acta 66 (2003) 3177.
[38] A. Andara, D.M. Heasman, A. Fernández-González, M. Prieto, Cryst. Growth Des. 5 (2005) 1371.
[39] P.E. Hillner, A.J. Gratz, S. Manne, P.K. Hansma, Geology 20 (1992) 359.
[40] S.L. Stipp, C.M. Eggleston, B.S. Nielsen, Geochim. Cosmochim. Acta 58 (1994) 3023.
[41] Y. Liang, A.S. Lea, D.R. Baer, M.H. Engelhard, Surf. Sci. 351 (1996) 172.
[42] G. Jordan, W. Rammensee, Geochim. Cosmochim. Acta 62 (1998) 941.
[43] A.A. Chernov, Modern Crystallography III: Crystal Growth, Springer Series in Solid-State Sciences, vol. 36, Springer-Verlag, Berlin, 1984 (Chapter 4).
[44] J.M. Astilleros, C.M. Pina, L. Fernández-Díaz, A. Putnis, Geochim. Cosmochim. Acta 67 (2003) 1601.
[45] W.M.M. Heijnen, Neues Jb. Miner. Mh. 8 (1985) 357.
[46] J. Paquette, R.J. Reeder, Geochim. Cosmochim. Acta 59 (1995) 735.
[47] W.J. Staudt, R.J. Reeder, M.A.A. Schoonen, Geochim. Cosmochim. Acta 58 (1994) 2087.
[48] R.J. Reeder, J. Rakovan, Surface structural controls on trace element incorporation during crystal growth, in: B. Jamtveit, P. Meakin (Eds.), Growth, Dissolution and Pattern Formation in Geosystems, Kluwer Academic Publishers, 1999, p. 143.
[49] G. Jordan, S.R. Higgins, C.M. Eggleston, K.G. Knauss, W. Schmahl, Geochim. Cosmochim. Acta 65 (2001) 4257.
[50] J. Ganor, A.C. Lasaga, Geochim. Cosmochim. Acta 62 (1998) 1295.
[51] S.G. Terjesen, O. Erga, G. Thorsen, A. Ve, Chem. Eng. Sci. 74 (1961) 277.
[52] M.B. Hay, R.K. Workman, S. Manne, Langmuir 19 (2003) 3727.
[53] A.S. Lea, J.E. Amonette, D.R. Baer, Y. Liang, N.G. Colton, Geochim. Cosmochim. Acta 65 (2001) 369.
[54] R.S. Arvidson, M. Collier, K.J. Davis, M.D. Vinson, J.E. Amonette, A. Luttge, Geochim. Cosmochim. Acta 70 (2006) 583.
[55] L.E. Wasylenki, P.M. Dove, D.S. Wilson, J.J. De Yoreo, Geochim. Cosmochim. Acta 69 (2005) 3017.
[56] R.J. Reeder, Geochim. Cosmochim. Acta 60 (1996) 1513.
[57] K.J. Davis, P.M. Dove, L.E. Wasylenki, J.J. De Yoreo, Am. Mineral. 89 (2004) 714.
[58] D.L. Parkhurst, C.A.J. Appelo, User's Guide to PHREEQC, US Geological Survey Water Resources Investigations Report 99-4259, US Geological Survey, Washington, DC, 1999.
[59] A.S. Lea, T.T. Hurt, A. El-Azab, J.E. Amonette, D.R. Baer, Surf. Sci. 524 (2003) 63.
[60] A.G. Shtukenberg, J.M. Astilleros, A. Putnis, Surf. Sci. 590 (2005) 212.
[61] H.C. Helgeson, Geochim. Cosmochim. Acta 32 (1968) 853.